

# Intermingled basins in coupled Lorenz systems

Sabrina Camargo <sup>1</sup>, Ricardo L. Viana <sup>2</sup>, and Celia Anteneodo <sup>1,3</sup>

<sup>1</sup> *Department of Physics, PUC-Rio, Rio de Janeiro, Brazil*

<sup>2</sup> *Department of Physics, Federal University of Paraná, Curitiba, Brazil*

<sup>3</sup> *National Institute of Science and Technology for Complex Systems, Rio de Janeiro, Brazil.*

(Dated: September 15, 2018)

We consider a system of two identical linearly coupled Lorenz oscillators, presenting synchronization of chaotic motion for a specified range of the coupling strength. We verify the existence of global synchronization and antisynchronization attractors with intermingled basins of attraction, such that the basin of one attractor is riddled with holes belonging to the basin of the other attractor and *vice versa*. We investigated this phenomenon by verifying the fulfillment of the mathematical requirements for intermingled basins, and also obtained scaling laws that characterize quantitatively the riddling of both basins in this system.

PACS numbers: 0.45.Xt,05.45.Df,05.45.Pq,05.45.-a

## I. INTRODUCTION

The Lorenz system

$$\dot{x} = \alpha(y - x), \quad \dot{y} = \beta x - y - xz, \quad \dot{z} = -\gamma z + xy, \quad (1)$$

for  $\alpha = 10$ ,  $\beta = 28$ , and  $\gamma = 8/3$ , displays a chaotic attractor with the familiar butterfly-like shape [1]. It is often quoted as a paradigmatic system in nonlinear dynamics, since it displays many interesting dynamical properties of chaotic dissipative systems. Moreover its equations mimetize the dynamical behavior expected to occur in some physically relevant systems, as convection rolls in the atmosphere [1], single-mode lasers [2], and segmented disk dynamos [3]. Coupled Lorenz systems could arise as well in the mathematical modeling of related physical problems. The simplest case in the latter category is the coupling of two identical Lorenz systems.

In identical coupled systems, even if chaotic, synchronization of trajectories may occur [4]. This phenomenon has been studied for more than two decades, motivating a wealth of analytical, numerical, and even experimental results [5]. Synchronization of chaos, besides its own interest as a mathematical problem, finds applications for instance in secure communications [6]. The chaotic nature of the dynamics of one of the systems can be exploited to code messages which could be sent to an identical system through some form of coupling. If the latter system is synchronized with the former, the message can be securely decoded.

For two completely synchronized systems, either periodic or chaotic, their dynamical variables are equal for all times. On the other hand, if instead of the difference, it is the sum of some of their dynamical variables that vanishes, the two systems are said to antisynchronize. Due to phase-space symmetries, coupled Lorenz systems can exhibit both synchronized and antisynchronized states. Then, for secure communications purposes, the existence of another, antisynchronized, state is in principle a source of troubles since, depending on the initial condition, the receiver system could be tuned to the antisynchronized

attractor. This situation can still be dramatically worsen when the riddling phenomenon occurs.

As a matter of fact, multistable dynamical systems typically have a very complicated structure of basins of attraction, that may be delimited by fractal boundaries [7]. Suppose, for instance, that a dynamical system has two attractors, with the corresponding basins of attraction sharing a common basin boundary in the phase space. If a ball centered at a given initial condition and with a radius equal to the uncertainty level intercepts the basin boundary, we cannot say *a priori* which attractor the system will asymptote to [8]. If that boundary is a curve, even if fractal, the final-state sensitivity problem can be circumvented by decreasing the radius of the uncertainty ball (this can be done in experimental or numerical settings, by increasing the precision in determining the initial condition in phase space). However, such reduction of uncertain initial conditions is not possible in the limit case in which the fractal boundary is area-filling, i.e., the (box-counting) dimension of the basin boundary gets close to the dimension of the phase space itself [9]. In that limit case, the fraction of uncertain initial conditions will likely not decrease no matter how much we decrease the uncertainty balls of each initial condition. The latter situation occurs for riddled basins [9].

From the mathematical point of view, riddled basins are observed in dynamical systems that exhibit an invariant smooth hypersurface with a chaotic attractor lying on it, another asymptotic final state, out of the invariant subspace, and negative Lyapunov exponent transverse to the invariant subspace with positive finite-time fluctuations [10–12]. Under the conditions above, riddling originates from the loss of transversal stability of unstable periodic orbits embedded in the chaotic attractor [13], despite the attractor being transversely stable in average. In this context, attractors must be understood in the weak sense of Milnor [14]. The transition associated to the first unstable orbit on the attractor that losses transversal stability determines the riddling bifurcation (see for instance Ref. [15] for an overview). Depending on the way these orbits loss stability and even on the

dynamics outside the invariant manifold, different bifurcation scenarios and different forms of riddled basins can occur [13, 16–18] (to cite a few examples).

If riddled basins exist in a multistable chaotic system, their final states are utterly unpredictable, i.e. we cannot say - with any degree of certainty - which attractor the system will evolve to for long times [19]. The situation, in this case, is similar to that for a random process, for which there can only be determined a probability for predicting the final state of the system. In fact, some phenomena formerly attributed to random variations in initial conditions can be also interpreted as a consequence of riddling [20].

The simplest case of riddling is when only one of the co-existing attractors have a riddled basin. However, when there is more than one invariant subspace, then more than one attractor can be riddled. In this case, the basin structure is called *intermingled* [9].

The aim of the present work is precisely to show the existence of intermingled basins of attraction for the synchronized and antisynchronized states of two coupled Lorenz oscillators. In previous literature there are already clues of such phenomenon. Kim and coworkers [21], in a work about anti-synchronization of coupled chaotic oscillators, point to the possibility of a riddled basin of synchronization in coupled Lorenz systems, but without going further on that issue. Furthermore, a one-dimensional reduction of the Lorenz system (to a piecewise approximation to the well-known Lorenz map) was low-dimensional enough for an analytical treatment to be feasible and show the riddling of the synchronization basin [22]. The verification of the transversal stability conditions through direct methods (i.e., by making a linear stability analysis of each invariant subspace) is quite difficult in two coupled Lorenz systems, since the phase space is six-dimensional. Then, we investigate those properties numerically. We also characterize quantitatively the riddled basins by means of the scaling laws giving the probability of making wrong predictions on the final state of the system, with respect to two quantities of interest: (i) the phase-space distance to the invariant subspace; and (ii) the uncertainty radius for each initial condition [23]. We have verified that, for both quantities, the probability scales as a power-law, as required for riddled basins.

The rest of the paper is organized as follows: Section II describes the coupled system of Lorenz oscillators, as well as the existence of both synchronized and antisynchronized states. Section III presents a preliminary discussion of the basins of attraction of both the synchronized and antisynchronized states. The mathematical properties required for riddled basins and the necessary tools are the object of Section IV. Section V discusses the quantitative characterization of riddled basins through scaling laws and the theoretical results supporting them. The last Section contains our conclusions and final remarks.

## II. COUPLED LORENZ SYSTEMS

Many different coupling schemes are possible for two identical Lorenz systems [24]. We have chosen, for symmetry reasons, a diffusive coupling through the  $z$ -variable, as follows

$$\begin{aligned}\dot{x}_1 &= \alpha(y_1 - x_1), \\ \dot{y}_1 &= \beta x_1 - y_1 - x_1 z_1, \\ \dot{z}_1 &= -\gamma z_1 + x_1 y_1 + \varepsilon(z_2 - z_1), \\ \dot{x}_2 &= \alpha(y_2 - x_2), \\ \dot{y}_2 &= \beta x_2 - y_2 - x_2 z_2, \\ \dot{z}_2 &= -\gamma z_2 + x_2 y_2 + \varepsilon(z_1 - z_2),\end{aligned}\tag{2}$$

where we will use the same values for  $\alpha$ ,  $\beta$ , and  $\gamma$ , as in the uncoupled case, and  $\varepsilon$  is the coupling strength.

On considering the dynamical behavior of the coupled system, it is convenient to perform the changes of variables

$$\begin{aligned}x &= \frac{(x_2 - x_1)}{2}, & y &= \frac{(y_2 - y_1)}{2}, & z &= \frac{(z_2 - z_1)}{2}, \\ X &= \frac{(x_2 + x_1)}{2}, & Y &= \frac{(y_2 + y_1)}{2}, & Z &= \frac{(z_2 + z_1)}{2},\end{aligned}\tag{3}$$

after which the coupled system (2) becomes

$$\begin{aligned}\dot{x} &= \alpha(y - x), \\ \dot{y} &= \beta x - y - (Xz + Zx), \\ \dot{z} &= -(\gamma + 2\varepsilon)z + Xy + Yx, \\ \dot{X} &= \alpha(Y - X), \\ \dot{Y} &= \beta X - Y - (XZ + xz), \\ \dot{Z} &= -\gamma Z + XY + xy.\end{aligned}\tag{4}$$

Whenever more convenient to the analysis, we will refer either to the new or the old variables.

From inspecting Eqs. (4) there follows that the dynamics of the coupled system is invariant with respect to the transformation  $(x, y, z) \rightarrow (-x, -y, -z)$ . Hence the conditions  $x = y = z = 0$  define an invariant subspace  $\mathcal{M}_s$ : one initial condition that belongs to this subspace generates a trajectory in phase space that remains in  $\mathcal{M}_s$  for any time. This three-dimensional subspace defines the complete (or global) synchronization manifold characterized by  $x_1 = x_2$ ,  $y_1 = y_2$ ,  $z_1 = z_2$ .

The dynamics in the invariant subspace  $\mathcal{M}_s$ , described by the variables  $(X, Y, Z)$ , is governed by the equations of the uncoupled Lorenz system, hence there is a chaotic attractor  $\mathcal{A}_s$  (butterfly-like shape) lying in  $\mathcal{M}_s$ .

Analogously, due to the symmetry  $(X, Y, z) \rightarrow (-X, -Y, -z)$ , the states for which  $X = Y = z = 0$  define another invariant subspace  $\mathcal{M}_a$  (anti-synchronization manifold), associated to the attractor  $\mathcal{A}_a$ , in which  $(x, y, Z)$  follows the dynamics of the uncoupled system, i.e.  $\mathcal{A}_a$  is a Lorenz chaotic attractor in  $\mathcal{M}_a$ .

There are also other symmetries already present in the uncoupled Lorenz system. Notice in Eqs. (2) that either  $(x_1, y_1) \rightarrow (-x_1, -y_1)$  or  $(x_2, y_2) \rightarrow (-x_2, -y_2)$  lead, to

four-dimensional invariant subspaces, while both symmetries together lead to a two-dimensional invariant subspace with a saddle point at the origin. Finally, included in this two-dimensional subspace, the lines at  $z_1 = z_2$  and  $z_1 = -z_2$  also represent invariant subsets. We did not find any other relevant attractor other than  $\mathcal{A}_s$  and  $\mathcal{A}_a$ , which are attractors of the dynamics in the respective subspaces  $\mathcal{M}_s$  and  $\mathcal{M}_a$ , and can become attractors for the whole phase space depending on their transversal stability.

### III. BASINS OF ATTRACTION

In dynamical systems with more than one attractor, the corresponding basins may have fractal boundaries and even more complicated structures like the Wada property [25]. Accordingly, in the coupled Lorenz system (2), the two coexisting attractors representing synchronized and antisynchronized states are expected to have such complex basin boundary structure.

Since the phase space of the coupled system is six-dimensional, the visualization of the basins of attraction depends on convenient phase space sections or projections. Figure 1 shows a section of the basin of the anti-synchronization (synchronization) attractor  $\mathcal{A}_a$  ( $\mathcal{A}_s$ ), for different values of the coupling parameter.

Each initial condition was integrated using a fourth-order Runge-Kutta scheme with fixed timestep  $10^{-3}$  and for a time  $t = 10^3$ , after which we determined to what attractor the corresponding orbit has asymptoted [26]. If an orbit has asymptoted to an antisynchronized (synchronized) state in  $\mathcal{M}_a$  ( $\mathcal{M}_s$ ), its initial condition was painted black (white). Hence the area painted black (white) is a numerical approximation of a section of the basin of attractor  $\mathcal{A}_a$  ( $\mathcal{A}_s$ ). We considered  $10^5$  initial conditions with  $x_1 = x_2 = y_1 = y_2 = 1.0$  while  $z_1$  and  $z_2$  were

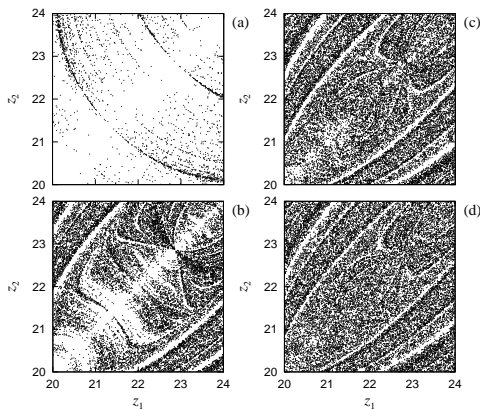


FIG. 1: Section at  $x_1 = x_2 = y_1 = y_2 = 1.0$  of the basins of synchronization (white pixels) and anti-synchronization (black pixels) attractors of the coupled Lorenz system, for  $\varepsilon =$  (a) 1.0, (b) 2.0, (c) 2.5 and (d) 2.8.

randomly chosen in the interval  $[20, 24)$  according to a uniform probability distribution.

For instance, for a coupling strength  $\varepsilon = 1.0$  [Fig. 1(a)], the section of the basin of attractor  $\mathcal{A}_a$  is a series of thin filaments stemming from the diagonal. The filaments are non-uniformly distributed and have a suggestive self-similar appearance. In fact, successive magnifications of [Fig. 1(a)] reveal similar patterns (see Ref. [21]). Such scenario is also observed for other values of  $\varepsilon$ , as illustrated in Fig. 1(b-d), even if some features change with  $\varepsilon$ , such as the relative area of each basin, or the definition of the tongues anchored in the diagonal. Let us note that other cuts also display a tongue structure, as depicted in Fig. 2 for  $\varepsilon = 2.0$ .

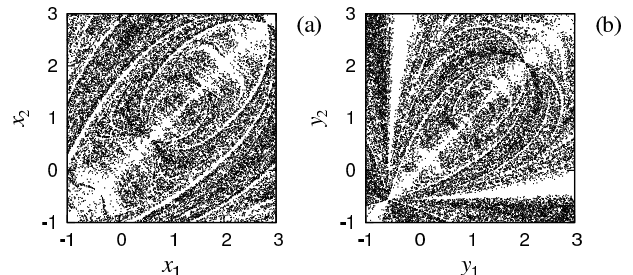


FIG. 2: Section at  $z_1 = z_2 = 22.0$  and (a)  $y_1 = y_2 = 1.0$ ,  $x_1, x_2$  random in  $[-1, 3)$ , (b)  $x_1 = x_2 = 1.0$ ,  $y_1, y_2$  random in  $[-1, 3)$  of the basins of synchronization (white pixels) and anti-synchronization (black pixels) attractors of the coupled Lorenz system, for  $\varepsilon = 2.0$ .

The structure of the basins of attraction is indeed expected to be altered by the coupling strength. As an example, in Fig. 3 we show that, for a given initial condition ( $x_1 = y_1 = z_1 = 1.0$  and  $x_2 = y_2 = z_2 = 0.5$ ) integrated up to time  $10^2$ , the trajectories in the subspace of each oscillator are distinct for  $\varepsilon = 0.5$ , while for  $\varepsilon = 1.0$  trajectories tend to coincide due to synchronization. In the latter case, the overlapping segments reproduce a cut of the familiar attractor of the single Lorenz system, since for synchronized orbits, the evolution proceeds towards the attractor in  $\mathcal{M}_s$  which is defined by  $x = y = z = 0$ , and  $X = x_1 = x_2$ ,  $Y = y_1 = y_2$ ,  $Z = z_1 = z_2$  follow the dynamics of an uncoupled system, as described above. Differently, in the former case ( $\varepsilon = 0.5$ ), the trajectories of each system depart from those of the uncoupled system.

Moreover, the observation of synchronized or antisynchronized states depends on the coupling strength. Recall that the existence of  $\mathcal{M}_s$  (i.e. the synchronized state being a possible solution of the coupled equations) does not mean necessarily that synchronized states, and in particular states in its attractor  $\mathcal{A}_s$ , can be observed in numerical simulations. This occurs only if there is transversal stability, in the sense that any infinitesimal displacement along directions transversal to  $\mathcal{M}_s$  decays exponentially with time.

Let us remark that, due to the symmetry of the equations with respect to synchronized/antisynchronized

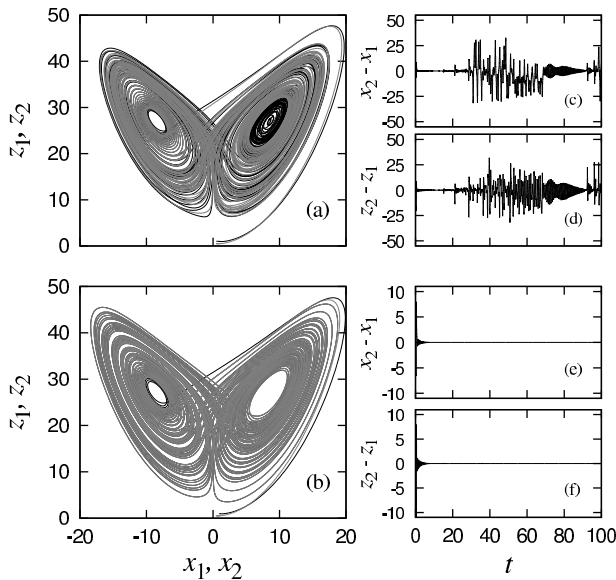


FIG. 3: Trajectories of the coupled Lorenz system for the same initial condition ( $x_1 = y_1 = z_1 = 1.0$  and  $x_2 = y_2 = z_2 = 0.5$ ) up to  $t = 100$  and different coupling values: (a)  $\varepsilon = 0.5$ ; (b) 1.0. In each case, the time evolution of the differences of coordinates are also shown (c)-(d) for  $\varepsilon = 0.5$  and (e)-(f) for  $\varepsilon = 1.0$ .

states, comments for attractor  $\mathcal{A}_s$  are also valid for  $\mathcal{A}_a$ .

In order to visualize the existence of a transversely stable synchronization manifold, we consider the differences  $x_1 - x_2$ ,  $y_1 - y_2$ , and  $z_1 - z_2$ , which must vanish if a synchronized attractor is achieved. For  $\varepsilon \gtrsim 0.7$ ,  $z_1 - z_2$  vanishes [Fig. 4(c)], while the other two differences may also vanish (global synchronization) or not (local synchronization) [Fig. 4(a) and (b)]. Similar plots are ob-

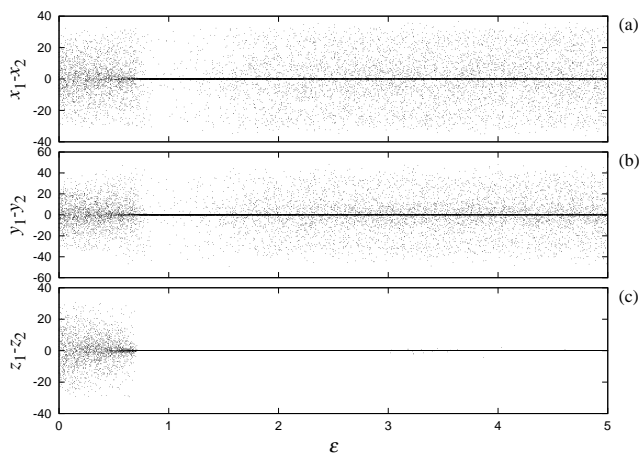


FIG. 4: Difference between the coordinates (a)  $x_1 - x_2$ ; (b)  $y_1 - y_2$ ; (c)  $z_1 - z_2$  of two coupled Lorenz systems at time  $t = 10^3$ , as a function of the coupling strength. One hundred initial conditions were randomly chosen (as in Fig. 1) for each value of  $\varepsilon$  (varied in steps of 0.01).

tained for the sums  $x_1 + x_2$ ,  $y_1 + y_2$ , indicating that the basins of the synchronized and antisynchronized states are complementary to each other.

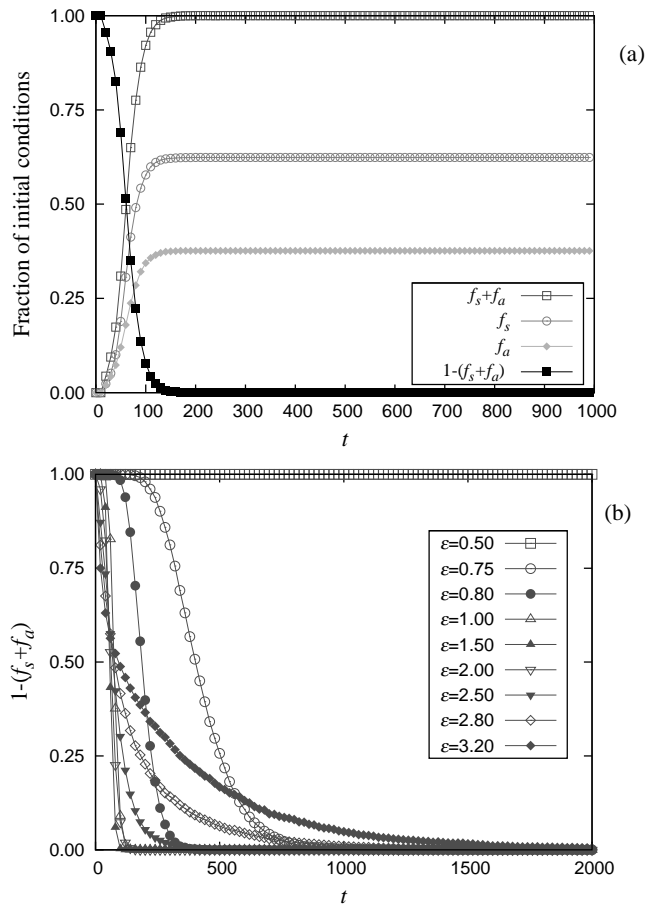


FIG. 5: (a) Fraction of initial conditions (over a total of  $10^4$ ) yielding trajectories asymptoting synchronized  $f_s$  or antisynchronized  $f_a$  states as a function of time, for  $\varepsilon = 2.0$ . We also indicated the fraction of trajectories reaching either state ( $f_s + f_a$ ) or none of them ( $1 - f_s + f_a$ ). (b) Fraction of initial conditions not reaching these states for different values of the coupling strength.

We did not find any relevant attractor for the coupled system other than  $\mathcal{A}_s$  and  $\mathcal{A}_a$ . Besides the symmetry considerations at the end of Sect. II, we performed the following numerical experiment: we considered the initial conditions used to plot the sections in Fig. 1 and, for each time  $t$  we computed the fraction of initial conditions that go either to  $\mathcal{A}_s$  or  $\mathcal{A}_a$  [Fig. 5(a)]. The sum of these fractions rapidly approaches 100% [Fig. 5(a)], meaning that the fraction of initial conditions that do not asymptote to them goes to zero (filled squares in Fig. 5(a)), suggesting the existence of only two attractors for the coupled system. This conclusion has been observed to hold for  $\varepsilon \gtrsim 0.7$  as illustrated in [Fig. 5(b)]. Otherwise, neither synchronized nor antisynchronized states are approached, as illustrated in Fig. 3(c)-(d) for  $\varepsilon = 0.5$ . (Therefore, basin diagrams as those shown in Fig. 1 will

be left blank).

#### IV. RIDDLED AND INTERMINGLED BASINS

The standard requirements for the existence of a riddled basin are the existence of (i) a smooth invariant subspace (of lower dimension than the phase-space) containing a chaotic attractor, (ii) another asymptotic final state (not necessarily chaotic) out of the invariant subspace, (iii) negativity of the Lyapunov exponents transverse to the invariant subspace with (iv) positive finite-time fluctuations [9–11], which are associated to the transversal stability properties of unstable periodic orbits (UPOs) embedded in the attractor. For two symmetrically intermingled basins, the requirements for mutual riddling can be summarized as follows:

1. There are invariant manifolds  $\mathcal{S}_s$  and  $\mathcal{S}_a$  contained in the phase space  $\mathcal{H}$ .
2. The dynamics on each manifold  $\mathcal{S}_{s,a}$  has a chaotic attractor.
3.  $\mathcal{S}_{s,a}$  are transversely stable, meaning that the largest transversal Lyapunov exponent  $\lambda_\perp$  is negative.
4. Although weak stability holds in average (condition 3), UPOs embedded in the chaotic attractor are transversely destabilized.

In Section III we showed that conditions 1 and 2 are fulfilled for the coupled Lorenz systems. There exists two (three-dimensional) manifolds,  $\mathcal{S}_{s,a} = \mathcal{M}_{s,a}$ , in the six-dimensional phase space. They are invariant since trajectories starting in each subspace will remain there forever. Because the dynamics in each subspace coincides with that of the uncoupled map, then, it will evolve towards the respective well known Lorenz attractor  $\mathcal{A}_{s,a}$  lying in the corresponding manifold.

Moreover, for each invariant subspace, there are out of three transversal directions. Condition 3 means that the transverse Lyapunov exponents of typical orbits lying in the invariant subspaces ( $\mathcal{M}_a$  and  $\mathcal{M}_s$ ) are all negative. The point in parameter space where they become positive defines the blowout bifurcation [11]. To investigate condition 3, it suffices to consider the largest transversal exponent, denoted as  $\lambda_\perp = \lim_{t \rightarrow \infty} \frac{1}{t} \ln \frac{\delta(t)}{\delta(0)} < 0$ , where  $\mathbf{x}_0$  is an initial condition on the basin of attraction of either  $\mathcal{A}_a$  or  $\mathcal{A}_s$ .

We computed Lyapunov exponents using two different methods. The Lyapunov spectrum was obtained following the algorithm of Wolf *et al.* [27], with a Gram-Schmidt normalization step of 0.1. We integrated Eqs. (2) using initial conditions given by  $x_1 = y_1 = x_2 = y_2 = 1.0$  and  $z_1, z_2$  were randomly chosen in the interval [20, 24) from a uniform probability function, as in Fig. 1. These initial conditions lead to trajectories that asymptote to either  $\mathcal{A}_s$  or  $\mathcal{A}_a$ . As a matter of fact, this is not

relevant since both attractors have the same Lyapunov spectrum.

The second method we used, and which can be applied to obtain only the largest transversal exponent, is to consider the time evolution of an infinitesimal displacement along a direction transversal to the synchronized subspace  $\mathcal{M}_s$ , which is given by [7],

$$\lambda_\perp = \lim_{t \rightarrow \infty} \frac{1}{t} \ln \frac{\delta(t)}{\delta(0)}, \quad (5)$$

where  $\delta(t) = \sqrt{(\delta x)^2 + (\delta y)^2 + (\delta z)^2}$  is the norm of the transverse displacement, whose evolution is given by the variational equations for  $(x, y, z)$ , setting  $x = y = z = 0$ , i.e.,

$$\begin{aligned} \dot{\delta x} &= \alpha(\delta y - \delta x), \\ \dot{\delta y} &= \beta \delta x - \delta y - X \delta z - Z \delta x, \\ \dot{\delta z} &= -(\gamma + 2\varepsilon) \delta z + X \delta y + Y \delta x, \\ \dot{X} &= \alpha(Y - X), \\ \dot{Y} &= \beta X - Y - XZ, \\ \dot{Z} &= -\gamma Z + XY. \end{aligned} \quad (6)$$

Figure 6 shows (in gray symbols) the three largest (infinite-time) Lyapunov exponents as a function of the coupling strength  $\varepsilon$ , obtained by means of the algorithm by Wolf *et al.*, and the largest transversal exponent given by (5) is indicated by a thick black line. One of the exponents is always zero, corresponding to displacements along the trajectory. The largest exponent is practically always equal to  $\sim 0.9$  and corresponds to the chaotic dynamics on  $\mathcal{A}_s$  ( $\mathcal{A}_a$ ). The third exponent is the largest transversal exponent which we focus our attention on, both methods being in good accord in the region of interest (as shown in Fig. 6). For the chaotic attractors in both synchronization and antisynchronization manifolds,

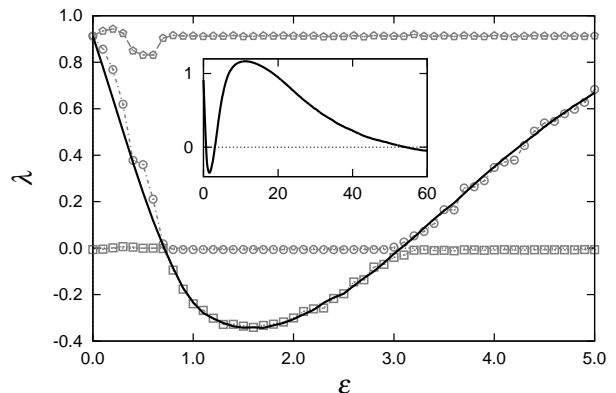


FIG. 6: The three largest Lyapunov exponents of the coupled Lorenz system as a function of the coupling strength. Gray symbols correspond to the algorithm by Wolf *et al.*, whereas the thick black curve is the result of the variational equations (6). Inset: the largest exponent for a wider range of  $\varepsilon$ .

the largest transversal exponent vanishes, changing sign, at  $\varepsilon_1 \approx 0.714 \pm 0.005$  and  $\varepsilon_2 \approx 3.061 \pm 0.005$ , defining the critical points of the blowout bifurcation. (There is also another critical value for large  $\varepsilon$ , as can be seen in the inset of Fig. 6, but we will restrict our analysis to the lower range only). The largest transversal exponent is negative for  $\varepsilon_1 < \varepsilon < \varepsilon_2$ , hence, in that interval, condition 3 for intermingled basins is fulfilled. However, while the invariant subspaces  $\mathcal{M}_{s,a}$  are stable in average, with negative transversal Lyapunov exponents, there may be particular unstable periodic orbits embedded in the chaotic attractors  $\mathcal{A}_{s,a}$  that are also transversely unstable, with positive largest transversal Lyapunov exponent [28] (condition 4). When trajectories come close to these unstable orbits, they will be repelled from the vicinity of the attractor. This will be reflected in positive values of the finite-time largest transversal Lyapunov exponent [10–12]. Then we numerically computed the finite-time largest transversal Lyapunov exponents  $\tilde{\lambda}_\perp(\mathbf{x}_0, t)$ , by means of Eq. (5) but at finite  $t$ . For large enough  $t$ , one recovers the infinite time exponent  $\lambda_\perp$ , which does not depend on  $\mathbf{x}_0$ , for almost all initial conditions in the attractors  $\mathcal{A}_{s,a}$ , in contrast to the finite-time ones that may depend on the initial condition.

We quantify the contributions of the finite-time largest transversal exponent by obtaining a numerical approximation to the corresponding probability distribution function  $P(\tilde{\lambda}_\perp(\mathbf{x}_0, t))$ . We considered a large number of points in  $\mathcal{M}_s$  (with  $x = y = z = 0$ ,  $X = Y = 1.0$ , and  $Z$  randomly chosen in the interval [20, 24]), and discarded a transient. These were the initial conditions used to compute the time- $t$  largest transversal Lyapunov exponents. Alternatively, we generated a single long chaotic trajectory (after the transient has elapsed) and divided it into time- $t$  segments, using then the ergodicity of the dynamics to ensure that the conditions are randomly chosen according to the natural measure of the attractor. The results were essentially the same.

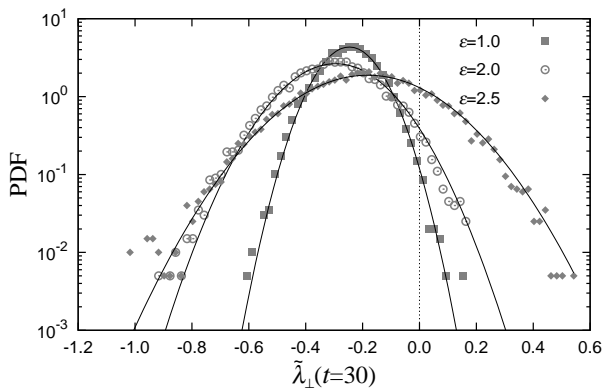


FIG. 7: Probability density functions of the time-30 largest transversal Lyapunov exponent for different values of  $\varepsilon$ . Initial conditions were taken as in Fig. 1. The full lines are Gaussian fits.

Figure 7 shows probability distribution functions (when  $t = 30$ ) for different values of the coupling strength. In all the considered cases the distribution is nearly Gaussian and presents positive tails. Then, we computed the positive fraction of finite-time exponents,  $\varphi(t) = \int_0^\infty P(\lambda_\perp(t)) d\tilde{\lambda}_\perp(t) > 0$ . The positive fraction is plotted in Fig. 8 as a function of the coupling strength for different values of the time- $t$  interval used to sample the finite-time exponents.

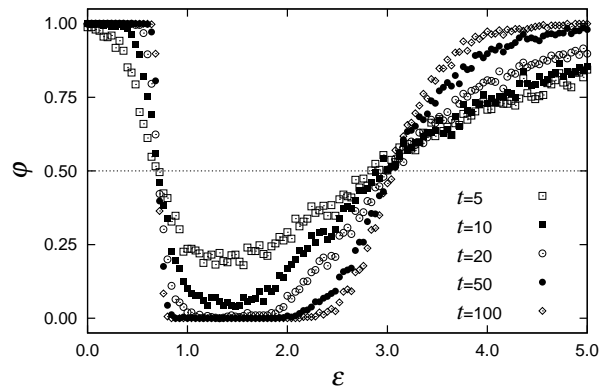


FIG. 8: Positive fraction of the largest time- $t$  transversal Lyapunov exponent as a function of the coupling strength, for different values of  $t$ .

For  $\varepsilon \lesssim \varepsilon_1$ , finite-time exponents soon become positive. This is in agreement with the positivity of the infinite-time exponent shown in Fig. 6 for this region, and also with the fact that trajectories do not approach the invariant subspaces, but are soon repelled, as already noted when we tried to plot the basins in Section III, which is not possible for that parameter range. The positive fraction drops rapidly to 50%, which corresponds to the case for which the infinite-time exponent vanishes (consistent with symmetric  $P(\tilde{\lambda}_\perp(t))$ ), and then drops below 50%, when the infinite-time exponent is negative. For  $\varepsilon \simeq 1.4$ , the positive fraction is minimal. For larger values of  $\varepsilon$ , it increases, crossing the 50% level again for  $\varepsilon \simeq \varepsilon_2$ , where the infinite-time exponent is again zero at that point (see Fig. 6). After that, the positive fraction tends to 1 gently with  $\varepsilon$ , yielding a positive infinite-time exponent. This smooth behavior, different from the abrupt one in the lower limit of the region of negative  $\lambda_\perp$ , is consistent with the observation, for  $\varepsilon > \varepsilon_2$ , of a basin structure reminiscent of those in Fig. 1, although the filaments from the diagonal are not neat. Even if trajectories are ultimately repelled, they can spend long time intervals close to each attractor.

The fraction of positive finite-time exponents is non-null. However, for the range  $\varepsilon_1 < \varepsilon < \varepsilon_2$ , that fraction decreases with  $t$ , as expected because the distribution of finite-time exponents collapses towards a Dirac delta centered at  $\lambda_\perp$  in the long time limit. The decay is exponential, the faster, the closer to the minimum at  $\varepsilon \simeq 1.4$ .

Hence, the absence of an abrupt decay of the positive fraction indicates a nonvanishing fraction for finite times. Then, from this analysis, condition 4 cannot be discarded for any range within the interval  $\varepsilon_1 < \varepsilon < \varepsilon_2$ . This suggests that at least one of UPOs should be transversely unstable in that interval.

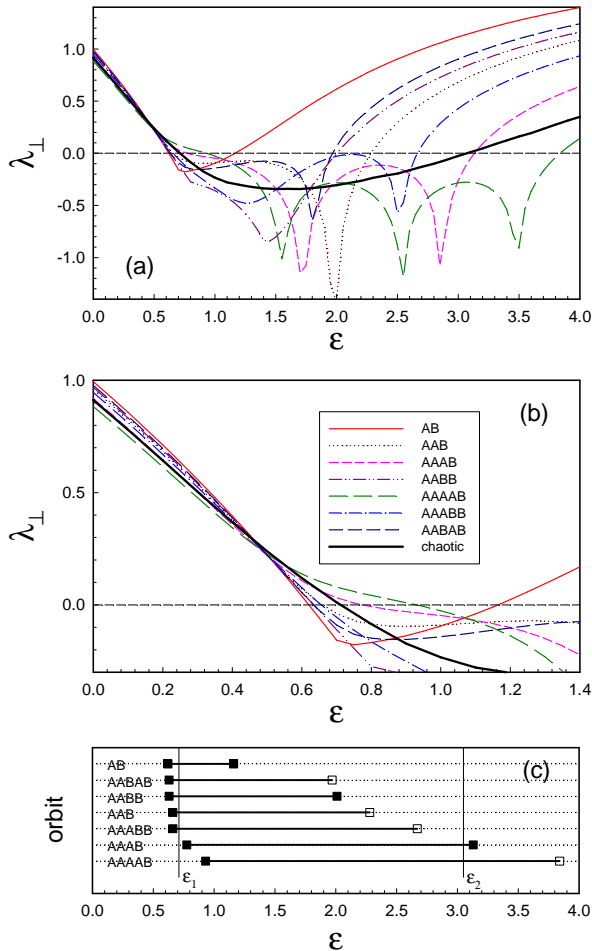


FIG. 9: (Color online) (a) Largest transversal Lyapunov exponent, as a function of  $\varepsilon$ , for the particular unstable periodic orbits (UPOs) embedded in the Lorenz chaotic attractor (up to period 5), indicated on the figure by means of the sequence of symbols A, B denoting the turns around each unstable fixed point  $C^+$  and  $C^-$  of the Lorenz system. The curve for typical chaotic trajectories in the attractor is also shown. (b) Magnification of panel (a). (c) Stability intervals for each UPO, in order of increasing stability at  $\varepsilon = 0$  from top to bottom: stable (full segment), unstable (dotted). The vertical lines indicate  $\varepsilon_1$  and  $\varepsilon_2$ . The symbols delimiting the stability intervals correspond to  $\mu = 1$  (full) and  $-1$  (hollow).

Then we inspected the transversal stability of those orbits along the lines of periodic orbits threshold theory [28]. Once localization in phase space and periods of low period UPOs are available in the literature for the Lorenz system [29], we computed Floquet multipliers [28, 30]. Namely, we integrated Eqs. (6), to obtain the matrix  $\mathbf{Q}$

such that  $\vec{\delta}(\tau) = \mathbf{Q}\vec{\delta}(0)$ , with  $\tau$  the time period of the orbit and  $\vec{\delta}(t) = (\delta x, \delta y, \delta z)$  the column vector of transverse deviations. The eigenvalue of  $\mathbf{Q}$ ,  $\mu$ , with maximal modulus furnishes  $\lambda_{\perp} = \ln |\mu|/\tau$ , for a particular periodic orbit. Fig. 9 shows the behavior of  $\lambda_{\perp}$  as a function of  $\varepsilon$  for particular UPOs, up to period 5. UPOs are labeled by means of the sequence of symbols A, B denoting the turns around each unstable fixed point  $C^+$  and  $C^-$  of the Lorenz system. Symmetric orbits obtained by exchanging  $A \leftrightarrow B$  or with cyclic symmetry were omitted.

One observes that the lowest period orbit AB (period 2) appears to be the first in destabilizing the vicinity of  $\varepsilon_2$ , hence defining a riddling bifurcation. Then, between this point and  $\varepsilon_2$  riddling can occur. This interval covers most of the range  $\varepsilon_1 < \varepsilon < \varepsilon_2$ , except for a very small interval in the vicinity of  $\varepsilon_1$ . However, note that orbits of the type  $A^n B$ , with  $n = 1, 2, \dots$ , have a maximal transversal Lyapunov exponents that increases with  $n$  in the vicinity of  $\varepsilon_1$ , hence shrinking the remaining small region of stability around  $\varepsilon \simeq 1$ . To confirm whether this region of strong stability (with no transversely unstable orbits) actually disappears would require the analysis of higher period orbits, a hard task for this system, since the number of UPOs increases exponentially with the integer period.

Near the blowout bifurcation at  $\varepsilon_1$ , the low-period UPOs (up to period 5) destabilize for coupling strength either weaker or stronger than the critical value, but close to it. Let us remark that, differently to the coupled Rössler system studied by Heagy et al. [28], here the ordering of the exponents of the lowest period orbits in the neighborhood of  $\varepsilon_1$  is inverted with respect to the uncoupled case as depicted in Fig. 9. This implies that paradoxically the most stable orbits in the attractor are those responsible for the transversal destabilization in this parameter region. A similar inversion occurs on some domains of the parameter space of a system of symmetrically coupled Rössler oscillators [15, 17]. This characteristic turns difficult the determination of the riddling bifurcation (first destabilized orbit) related to the blowout at  $\varepsilon_1$ , apparently triggered by higher period orbits.

Furthermore, our outcomes point to a different nature of the blowout bifurcations at  $\varepsilon_1$  and  $\varepsilon_2$ . Nearby  $\varepsilon_1$ , UPOs destabilize in its vicinity. Moreover, for all the analyzed orbits, the multiplier  $\mu$  crosses the circle  $|\mu| = 1$  along the real positive semi-axis (associated to a pitchfork bifurcation). This is in contrast to the scenario at  $\varepsilon_2$ , where there are orbits destabilizing far from  $\varepsilon_2$  and with multiplier  $\mu$  either  $+1$  or  $-1$ . In particular, the first orbit AB loses stability with  $\mu = 1$ . The differences are consistent with the picture given by finite-time exponents, for instance in connection with Fig. 8, where a much abrupt behavior of the positive fraction was encountered near  $\varepsilon_1$ .

The intervals where riddling can occur are delimited on one side by the blowout bifurcation and on the other by the riddling bifurcation. In our case there are two of such

intervals and they apparently overlap, such that at least one UPO has lost transversal stability in the full range  $\varepsilon_1 < \varepsilon < \varepsilon_2$ , although this would have to be confirmed by the analysis of high period orbits, it is supported by the analysis of finite-time Lyapunov exponents.

## V. SCALING LAWS FOR RIDDLED BASINS

In this Section, we will focus on the determination of the scaling properties of the basins, which provide a measure of their structure[10]. Let us focus on the black filaments in Fig. 1(b), which belong to the basin of the antisynchronization attractor. They are anchored at the diagonal line, which is a cut of the synchronization manifold  $\mathcal{M}_s$ , given by  $x = y = z = 0$  and containing a chaotic attractor  $\mathcal{A}_s$ , while the antisynchronization attractor  $\mathcal{A}_a$  lies elsewhere. In Fig. 10(a) we portrait a schematic picture of that structure. The filaments of the basin of  $\mathcal{A}_a$  are tongues anchored at points of  $\mathcal{A}_s$ , and the complement of the filament set belongs to the basin of  $\mathcal{A}_s$ . If an initial condition starts within any of these narrow tongues, even if it is very close to  $\mathcal{A}_s$ , the resulting trajectory will asymptote to the other attractor.

The set of basin filaments for  $\mathcal{A}_a$  is expected to be self-similar by quite general grounds. Once the riddling bifurcation occurs for a given periodic orbit, it also occurs for every preimage of this orbit, yielding a dense set of tongue-like sets anchored at the corresponding preimages on  $\mathcal{A}_s$ . The tongue-like shape is a consequence of the nonlinear terms in the equations describing the transversal dynamics. The characteristic feature of riddling is that those tongues have widths that tend to zero as we approach  $\mathcal{A}_s$ . Hence the basin of  $\mathcal{A}_s$  always contains pieces of the basin of the other attractor, regardless the transversal distance to  $\mathcal{A}_s$ , so forming a fine structure of basin filaments (the same applying to  $\mathcal{A}_a$ ).

This fine structure can be quantitatively characterized by the following numerical experiment [11, 23]: let us consider the invariant manifold at  $x = y = z = 0$  and, depart from that manifold, for instance, by increasing  $z$ , up to a distance  $l = 2|z| \equiv |z_1 - z_2|$  [as depicted by the red line segment in Fig. 10(a)]. Then we evaluate the fraction  $V_l$  of points in that segment that belongs to the basin of  $\mathcal{A}_s$ . We obtained a numerical approximation of this fraction by considering a number of initial conditions  $x = y = 0$ ,  $|z| = l/2$ ,  $X = Y = 1.0$ , and  $Z$  randomly chosen in the interval  $[20, 24)$ . If the trajectories did not synchronize (within a small tolerance) up to a time such that transients have elapsed and stationarity holds (typically,  $t = 10^3$ ), we consider that they asymptote to the antisynchronization attractor  $\mathcal{A}_a$  and, accordingly, they do not belong to the basin of  $\mathcal{A}_s$ . If the latter is riddled with tongues belonging to the basin of  $\mathcal{A}_a$ , for any distance  $l$  (no matter how small) there is always a nonzero value of  $V_l$ . This fraction tends to zero as  $l \rightarrow 0$ . The fraction of length belonging to the basin of  $\mathcal{A}_a$  (fraction of trajectories that do not synchronize) can be written as

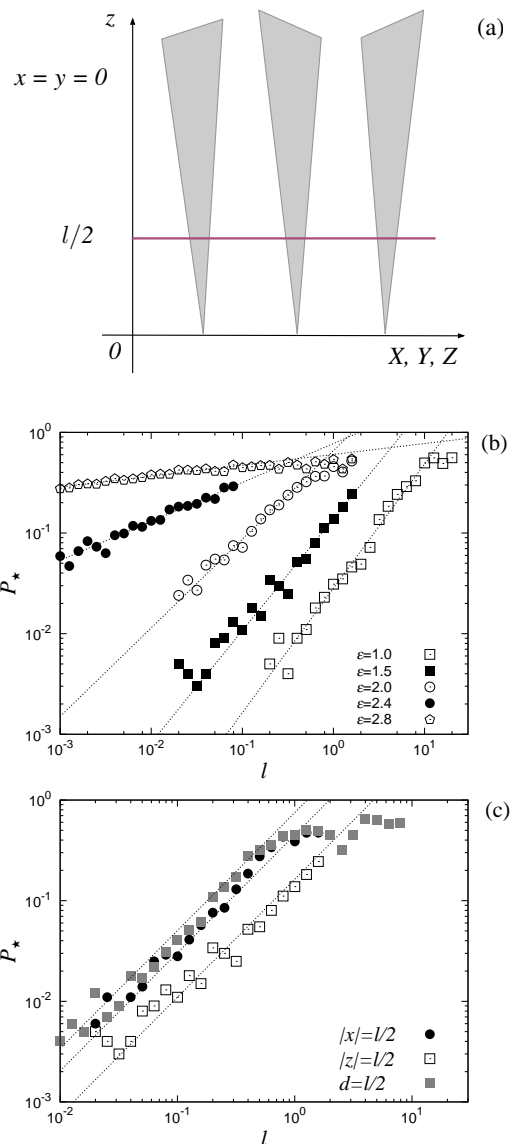


FIG. 10: (a) Schematic figure showing the structure of riddled basins near the invariant subspace that contains a chaotic attractor. (b) Fraction of trajectories  $P_*$  that asymptote to the antisynchronized state as a function of the distance  $l = 2|z|$  to the synchronized state, for different values of the coupling strength  $\varepsilon$ . The full lines are least squares fits. (c)  $P_*$  for  $\varepsilon = 1.5$  and different orientations of the deviation  $l$ .

$P_* = 1 - V_l$ , and is expected to scale with  $l$  as a power law  $P_*(l) \sim l^\eta$ , where  $\eta > 0$  is a scaling exponent. We integrated several initial conditions at the same distance  $l$  to the synchronization subspace and computed the fraction  $P_*$  of initial conditions that do not synchronize, repeating this procedure varying the distance  $l$ . The results shown in Fig. 10(b) confirm the existence of a power law for this fraction, for many values of the coupling strength.

The results do not vary appreciably when one departs from the synchronization manifold in other directions other than  $z$ . In Fig. 10(c) we plotted, for the same coupling strength ( $\varepsilon = 1.5$ ), the fraction  $P_*$  for initial

conditions with  $|z| = l/2$ ,  $x = y = 0$  (open squares), and also for  $|x| = l/2$ ,  $y = z = 0$  (filled circles) and random values of  $x, y, z$  such that  $d \equiv \sqrt{x^2 + y^2 + z^2} = l/2$  (filled squares), obtaining essentially the same scaling exponent. This scaling behavior is observed within the interval  $(\varepsilon_1, \varepsilon_2)$ , below  $\varepsilon_1$ , no trajectories synchronize as seen in the previous sections, above  $\varepsilon_2$ , one observes a synchronized fraction but it does not change with  $l$ . The dependence of the numerically determined scaling exponents  $\eta$  on the coupling strength is depicted in Fig. 11.

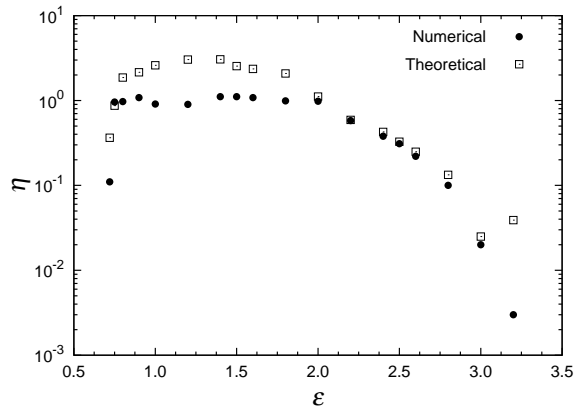


FIG. 11: Scaling exponent  $\eta$  for the fraction of trajectories that asymptote to the antisynchronized state obtained by a numerical experiment (filled circles). For comparison, the theoretical values, given by  $\eta = |\lambda_{\perp}|/D$  are also plotted (open squares).

An analytical expression for the exponent  $\eta$  was derived by Ott and coworkers for a simple model (piecewise linear non-invertible map) [23]. Their theoretical prediction arises from a diffusion approximation for a biased random walk that mimics the fluctuations of finite-time largest transversal Lyapunov exponents  $\lambda_{\perp}(t)$ . They obtain the law  $P_{\star} \sim l^{\eta}$ , with  $\eta = |\lambda_{\perp}|/D$  where  $D$  is the diffusion coefficient. This diffusion approximation is expected to be valid near the blowout bifurcation ( $\lambda_{\perp} \simeq 0$ ) of an attractor with a riddled basin. The authors conjecture that a similar diffusion approximation, hence a similar relation involving parameters  $\lambda_{\perp}$  and  $D$ , must rule the scaling relation in a large class of systems. The distributions shown in Fig. 7 already display a Gaussian character, which improves with larger time- $t$  interval, consistent with the probability distribution function of independent random innovations, that, by the central limit theorem, is Gaussian. Additionally, we plot in Fig. 12 the variance  $\sigma_{\lambda_{\perp}(t)}^2$  of the probability distribution functions for  $\lambda_{\perp}(t)$  as a function of time, for different values of the coupling strength. As a matter of fact, the variance decays with time towards zero following asymptotically a power-law with exponent  $-1$ , as required for a normal diffusion processes, so validating the stochastic approach of Ott *et al.* Accordingly, the diffusion coefficient  $D$  can be estimated from the numerical curves, following  $\sigma_{\lambda_{\perp}(t)}^2 \sim 2D/t$ . The

estimates  $\eta = |\lambda_{\perp}|/D$  are plotted in Fig. 11 together with the numerical values. Numerical and estimated values are in very good agreement in the proximity of the critical values, as expected [34]. For intermediate values ( $0.75 < \varepsilon < 2$ ) there is a discrepancy, and the numerical exponent remains close to one (linear behavior), as also observed for other systems with intermingled basins [20].

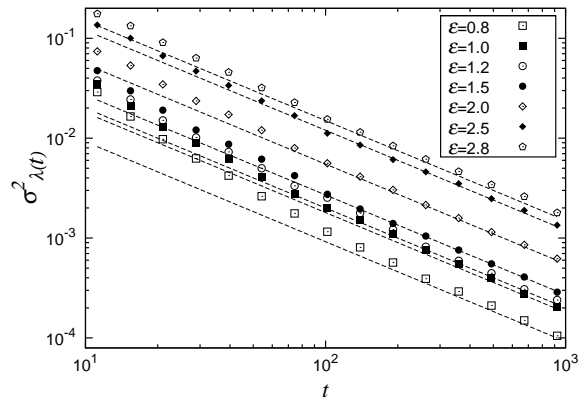


FIG. 12: Time decay of the variance of the finite-time largest transversal Lyapunov exponent for different values of the coupling strength  $\varepsilon$ . The lines are least squares fits of the function  $f(t) = 2D/t$  to the numerical points, for large  $t$ , allowing to estimate the diffusion coefficient  $D$ .

Another scaling law typical of riddled basins is related to the fraction of uncertain initial conditions, with respect to their final-state [31]. We may regard riddled basins as an extreme case of fractal basins, for which there is final-state sensitivity and the uncertainty fraction scales as a power-law with the uncertainty level, whose exponent gives a measure of the extreme final-state sensitivity due to riddling. Consider again the points at  $x = y = 0$  and  $|z| = l/2$  drawn in the phase space portrait in Fig. 13(a), as described earlier, and choose randomly an initial condition  $\mathbf{x}_0$  on that region. Now choose randomly another initial condition  $\mathbf{x}'_0$  with uniform probability within an interval of length  $2\xi$  and centered at  $\mathbf{x}_0$  [Fig. 13(a)]. If both points belong to different basins, they can be referred to as  $\xi$ -uncertain [32, 33].

The fraction of  $\xi$ -uncertain points, or uncertainty fraction, denoted by  $\langle p \rangle$ , is the probability of making a mistake when attempting to predict which basin the initial condition belongs to, given a measurement uncertainty  $\xi$ . This probability scales with the uncertainty level as a power law of the form  $\langle p \rangle \sim \xi^{\phi}$ , where  $\phi \geq 0$  depends on both  $\mathbf{x}_0$  and  $l$ . Numerical results are shown in Fig. 13(b). The stochastic model of Ott *et al.* predicts a power-law, with exponent given by  $\phi = \lambda_{\perp}^2/(4D\lambda_{\parallel})$ , a prediction that agrees with our numerical results close to the critical points. However, for intermediate values, while the stochastic model predicts small (though nonzero) values ( $\phi < 0.28$ ), our numerical results for  $\phi$ , as illustrated in Fig. 13(b), yield much smaller values (by a factor greater than ten). As a matter of fact, for riddled basins, the ex-

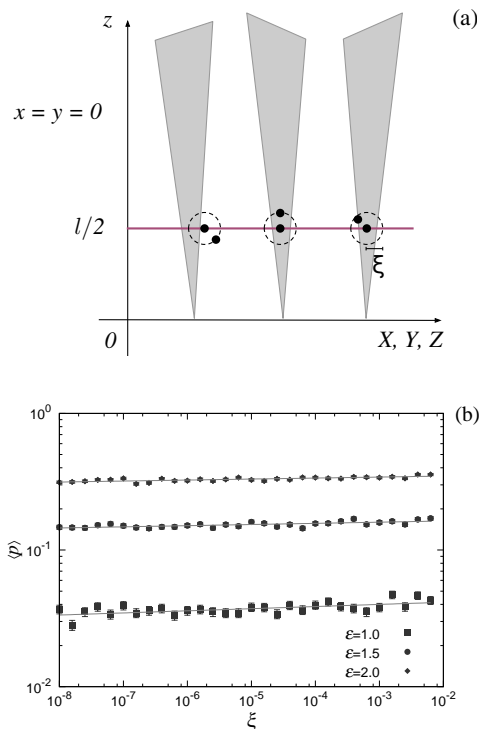


FIG. 13: (a) Schematic figure showing the numerical determination of the uncertainty fraction. (b) Fraction of uncertain initial conditions as a function of the uncertainty level, for different values of the coupling strength. The solid lines are least squares fits.

ponent  $\phi$  should be rigorously zero (i.e. there would be no way to decrease the uncertainty fraction by decreasing the uncertainty level). Indeed, our results [Fig. 13(b)] support this scaling law, with numerically obtained exponents close to zero.

## VI. CONCLUSIONS AND FINAL REMARKS

Riddled basins for the synchronization attractor of coupled Lorenz systems have been previously suggested in the literature but without a detailed characterization. In this work we offer numerical evidence that, for a specified range of the coupling parameter ( $\varepsilon_1 < \varepsilon < \varepsilon_2$ ), coupled Lorenz systems exhibit symmetrically riddled basins of attraction for synchronized and antisynchronized states. Since there are only two symmetric attractors, their basins are intermingled. We firstly showed that the mathematical conditions for the existence of riddled basins are fulfilled, with the help of properties of finite-time largest transversal Lyapunov exponents and of the largest transversal exponent for particular or-

bits. This is important as furnishes the sources of local transversal instability of the attractor even if stable in average. In a second place, we verified the existence of two scaling laws characterizing quantitatively the degree of uncertainty related to the riddled basins. These numerical results were compared to an analytical prediction (the stochastic model [23]), yielding a good accord where expected. Beyond the characterization of the structure of a riddled basin, these scaling laws allow to quantify the limitations to improve the ability in determining the final state of the system by increasing the accuracy level.

Let us remark that intermingling, in particular of symmetric basins, has also been observed in other systems with either continuous (e.g., mechanical system [12] and coupled Rössler oscillators[17]) or discrete time dynamics (coupled logistic maps [18]). In the latter case, the analysis of the lowest period orbit was enough to furnish the conditions for the occurrence of riddling in certain parameter region. In fact, as anticipated by the results presented in Fig. 9, deepening in that point of view may furnish precise information on the nature of the bifurcations triggering riddling, although this may be a difficult task for the present system. As other perspectives for future work on this system, let us also mention the plausible occurrence, beyond the blowout bifurcation, of two-state on-off intermittency [12] for which there is some evidence [21]. Finally, it can still be worthy to explore other regions of phase space, as well as other ranges (negative or large values) of the coupling parameter.

In any case, for applications, multistability is already a source of troubles. Still worst, the existence of intermingled basins of attraction for the synchronized and antisynchronized chaotic states of this system jeopardizes the solution of the problem of ensuring a given final state, since the initial condition determination is always done within a certain uncertainty level. With riddled basins, any uncertainty level, however small, lead to complete indeterminacy of the future state of the system. Hence in this case we cannot use synchronization of chaos for any practical purpose, since we will always be haunted by the existence of the another, antisynchronized state, with a basin intermingled with the basin of the synchronized state. Of course, the same difficulties concern the predictability of natural phenomena modeled by coupled Lorenz systems. Therefore, the importance of detecting the regimes where riddling can occur in a dynamical system.

## Acknowledgements:

This work was made possible with help of CNPq, CAPES, FAPERJ, and Fundação Araucária (Brazilian Government Agencies).

[1] E. N. Lorenz, J. Atmosph. Sci. **20**, 130 (1963).

[2] H. Haken, Phys. Lett. A **53**, 77 (1975).

- [3] E. Knobloch, Phys. Lett. A **82**, 439 (1981); I.M. Moroz, Proc. R. Soc. A **468**, 288 (2012).
- [4] H. Fujisaka, T. Yamada, Progr. Theoret. Phys. **69**, 32 (1983); L.M. Pecora, T.L. Carroll, Phys. Rev. Lett. **64**, 821 (1990).
- [5] A. Pikowsky, M. Rosenblum, and J. Kurths *Synchronization: a Universal Concept in Nonlinear Sciences* (Cambridge: Cambridge University Press, 2003).
- [6] K. Cuomo and A.V. Oppenheim, Phys. Rev. Lett. **71**, 65 (1993); M. Sushchik, N. Rulkov, L. Larson, L. Tsimrin, H. Abarbanel, K. Yao, A. Volkovskii, Comm. Lett. IEEE **4** 128 (2000).
- [7] J. Aguirre, R. L. Viana, and M. A. F. Sanjuán, Rev. Mod. Phys. **81**, 333 (2009).
- [8] C. Grebogi, E. Ott, and J. A. Yorke, Physica D **7**, 181 (1983).
- [9] J. C. Alexander, J. A. Yorke, Z. You, and I. Kan, Int. J. Bifur. Chaos **2**, 795 (1992).
- [10] E. Ott, J. C. Sommerer, J.C. Alexander, I. Kan and J.A. Yorke, Phys. Rev. Lett. **71**, 4134 (1993).
- [11] E. Ott and J. C. Sommerer, Phys. Lett. A **188**, 39 (1994).
- [12] Y.-Ch. Lai and C. Grebogi, Phys. Rev. E **52**, R3314 (1995).
- [13] Y.-Ch. Lai, C. Grebogi, J.A. Yorke, and S.C. Venkataramani, Phys. Rev. Lett. **77**, 55 (1996).
- [14] An attractor is the limit set of orbits from a set of initial conditions whose volume in phase-space is non-null. J. Milnor, Commun. Math. Phys. **99** 177 (1985).
- [15] S. Yanchuk, Y. Maistrenko, E. Mosekilde, Chaos **13**, 388 (2003).
- [16] P. Ashwin, J. Buescu, and I.N. Stewart, Phys. Lett. A **193**, 126 (1994).
- [17] S. Yanchuk, Y. Maistrenko, E. Mosekilde, Physica D **154**, 26 (2001); S. Yanchuk, Y. Maistrenko, B. Lading, E. Mosekilde, Int. J. Bifurc. Chaos **10**, 1051 (2000).
- [18] Yu. L. Maistrenko, V. L. Maistrenko, A. Popovich and E. Mosekilde, Phys. Rev. E **57**, 2713 (1998);
- [19] J. C. Sommerer, Apl. Tech. Dig. **16**, 333 (1995).
- [20] R. F. Pereira, S. Camargo, S. E. de S. Pinto, S. R. Lopes, and R. L. Viana, Phys. Rev. E **78**, 056214 (2008).
- [21] C.-M. Kim, S. Rim, W.-K. Kye, J.-W. Ryu, and Y.-J. Park, Phys. Lett. A **320**, 39 (2003).
- [22] M. C. Vergés, R. F. Pereira, S. R. Lopes, R. L. Viana, and T. Kapitaniak, Physica A **388**, 2515 (2009).
- [23] E. Ott, J. C. Alexander, I. Kan, J. C. Sommerer, and J. A. Yorke, Physica D **76**, 384 (1994).
- [24] R. Karnatak, R. Ramaswamy, and A. Prasad, Phys. Rev. E **76**, 035201 (2007).
- [25] H. E. Nusse, J. A. Yorke, Science **271**, 1376 (1996).
- [26] Notice that, due to the own nature of the basins, there are hindrances to determine them numerically. We considered that an orbit asymptotes to the attractor  $\mathcal{A}_s$  ( $\mathcal{A}_a$ ) if  $|x|, |y|, |z| < 10^{-8}$  ( $|X|, |Y|, |z| < 10^{-8}$ ) and verified that the resulting picture is not altered for later times.
- [27] A. Wolf, J. B. Swift, H. L. Swinney, and J. A. Vastano, Physica D **16**, 285 (1985).
- [28] J. F. Heagy, T.L. Carroll and L.M. Pecora, Phys. Rev. E **52**, R1253 (1995).
- [29] D. Viswanath, Nonlinearity **16** 1035 (2003); V. Franceschini, C. Giberti and Z. Zhengi, Nonlinearity **6** 251 (1993); Z. Galias, W. Tucker, in Proc. IEEE Int. Symposium on Circuits and Systems, ISCAS'08, 764 (2008).
- [30] A. Trevisan, F. Pancotti, J. Atm. Sci. **55** 390 (1997).
- [31] S. Camargo, S. R. Lopes and R. L. Viana, J. Phys. Conf. Series **246**, 012001 (2010).
- [32] C. Grebogi, S. W. McDonald, E. Ott, and J. A. Yorke, Phys. Lett. A **100** 1 (1985).
- [33] S. W. McDonald, C. Grebogi, E. Ott, and J. A. Yorke, Physica D **17** 125 (1985).
- [34] Y.-Ch. Lai and V. Andrade, Phys. Rev. E **64**, 056228 (2001).